Directional shear flow and Rho activation prevent the endothelial cell apoptosis induced by micropatterned anisotropic geometry

Chia-Ching Wu*†, Yi-Shuan Li*, Jason H. Haga*, Roland Kaunas*, Jeng-Jiann Chiu‡, Fong-Chin Su†, Shunichi Usami*, and Shu Chien*§

*Department of Bioengineering and Whitaker Institute of Biomedical Engineering, University of California at San Diego, La Jolla, CA 92093; †Institute of Biomedical Engineering, National Cheng Kung University, Tainan 701, Taiwan; and ‡Division of Medical Engineering Research, National Health Research Institutes, Miaoli 350, Taiwan

Contributed by Shu Chien, November 10, 2006 (sent for review October 17, 2006)

To study the roles of anisotropic cell morphology and directionality of mechanical force in apoptosis, the spreading of human umbilical vein endothelial cells (HUVECs) was constrained by growing on micropatterned (MP) strips of fibronectin (FN, 20 μg/cm^2) with widths of 15, 30, and 60 μm on silicone membrane. Cells on 30- and 60-μm strips, like cells on a nonpatterned (NP) surface coated with FN, showed clear actin stress fibers with anchoring spots of phosphorylated focal adhesion kinase (*p*-FAK) and no significant apoptosis. On 15-μm strips, cells had few stress fibers, no *p*-FAK, and significant apoptosis. After seeding for 12 h, the cells were subjected to pulsatile shear stress (12 ± 4 dyn/cm^2) parallel or perpendicular to MP strips, or kept under static condition. Parallel flow caused cell elongation with enhanced stress fibers and *p*-FAK, and a reduction in apoptosis, but perpendicular flow did not. The Rho inhibitory C3 exoenzyme abolished the effects of parallel flow. RhoV14, the constitutively active Rho, enhanced stress fibers and *p*-FAK, and prevented apoptosis of HUVECs on 15-μm strips under static condition. RhoV14 also reduced cell apoptosis under both parallel and perpendicular flows. Our results indicate that cell apoptosis can be modulated by changes in ECM micropatterning, anisotropic cell morphology, and mechanical forces. These extracellular microenvironment factors affect cell survival through alterations in Rho GTPase activity, stress fiber organization, and FAK phosphorylation.

actin stress fibers | focal adhesion kinase | micropatterning | Rho GTPase | shear stress

The regulation of survival and death of endothelial cells (ECs) is critical to vascular homeostasis. Perturbations of this balance contribute to vascular diseases (1). Apoptosis is a process for orderly disposal of unwanted cells and is necessary for homeostasis. It has been shown that modulation of the geometry of extracellular matrix (ECM) affects cell spreading and adhesion under static condition, thus modifying EC growth, differentiation, migration, and/or apoptosis (2). Microfabrication techniques have been used to investigate and control cell functions. Chen *et al*. (2) found that cell fate can be switched from proliferation to apoptosis by decreasing the size of the microfabricated ECM islands with a symmetric geometry.

Vascular ECs at the blood–vascular interface are constantly exposed to hemodynamic forces. It has been shown that the shear stress due to flow in straight parts of the vascular tree upregulates the genes involved in anti-apoptosis, cell cycle arrest, and morphological remodeling, thus contributing to atheroprotective effects (for review, see ref. 3). Such cell remodeling processes require both biochemical signaling and structural reorganization in response to the flow direction. There have been many reports on the role of ECM microenvironment in regulating cell morphogenesis and mechanotransduction in relation to vascular development and cardiovascular physiology (4), but the effects of changes in cell morphological constraints, especially their interplays with shear stress, are not well understood. The aim of the present study was to explore how ECs integrate the morphological and mechanical cues to modulate signal transduction and prevent the apoptotic consequence.

Microfabrication has been used to create polydimethylsiloxane (PDMS) molds for the preparation of anisotropically micropatterned (MP) strips of fibronectin (FN; 20 μg/cm^2) with different widths on silicone membrane to control cell orientation and adhesion area, thereby constraining the direction of cell remodeling (5). We applied shear flow to human umbilical vein endothelial cells (HUVECs) cultured on MP strips in directions parallel or perpendicular to the strips. We determined cell morphology and fate (apoptosis) as a function of strip width (15- to 60-μm). Flow in either direction enhanced intracellular formation of actin stress fibers and phosphorylated focal adhesion kinase (*p*-FAK). However, only parallel, but not perpendicular, flow can counter the apoptosis induced by culturing ECs on 15-μm strips.

In view of the important role played by Rho GTPase in regulating actin dynamics and FAK phosphorylation, we studied the role of Rho in the cell remodeling-dependent apoptosis and the underlying mechanisms. The Rho inhibitor C3 exoenzyme increased apoptosis of ECs seeded on 15-μm strips under static condition and abolished the anti-apoptotic effect of parallel flow. The constitutively active RhoV14 enhanced stress fiber formation and *p*-FAK, and attenuated apoptosis under static condition and under flows in either parallel or perpendicular direction. These findings provide insights into the mechanisms of cell apoptosis induced by anisotropic morphological constraint and its prevention or reversal by alterations in mechanical forces and intracellular signaling.

Results

Anisotropic Constraint Caused Endothelial Apoptosis. We proposed that the effective mechanical stress sensed by cells depends on cell morphology and remodeling. MP strips with widths of 15, 30, and 60 μm were created on a silicon membrane by using a PDMS

Author contributions: C.-C.W., Y.-S.L., J.H.H., R.K., J.-J.C., F.-C.S., S.U., and S.C. designed research; C.-C.W., J.H.H., and R.K. performed research; J.-J.C. and S.U. contributed new reagents/analytic tools; C.-C.W., Y.-S.L., J.H.H., R.K., J.-J.C., F.-C.S., and S.C. analyzed data; and C.-C.W., Y.-S.L., and S.C. wrote the paper.

The authors declare no conflict of interest.

Abbreviations: EC, endothelial cell; HUVEC, human umbilical vein endothelial cell; ECM, extracellular matrix; FN, fibronectin; MP, micropatterned; NP, nonpatterned; PDMS, polydimethylsiloxane; FA, focal adhesion; FAK, focal adhesion kinase; *p*-FAK, phosphorylated FAK; RhoV14, constitutively active form of Rho.

§To whom correspondence should be addressed at: Department of Bioengineering, University of California at San Diego, 9500 Gilman Drive, La Jolla, CA 92093-0412. E-mail: shuchien@ucsd.edu.

This article contains supporting information online at www.pnas.org/cgi/content/full/0609806104/DC1.

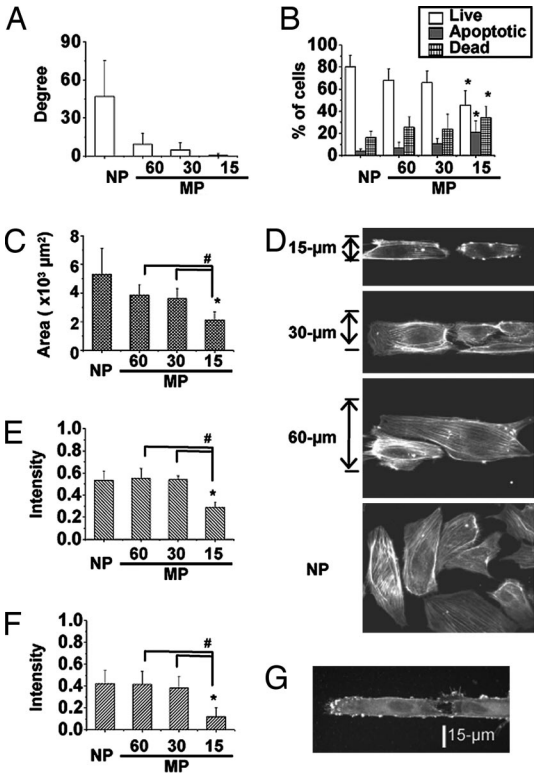

Fig. 1. Effects of anisotropic constraint on EC apoptosis. (*A*) With narrowing in width by micropatterned (MP) strips, the cell orientation became increasingly aligned parallel to the long axis of the strips as compared with the randomly orientated HUVECs on the nonpatterned (NP) surface. (*B*) The cell fate was analyzed by flow cytometry by using Annexin V and PI staining. Cells cultured on 15-μm strips (MP-15) showed a significantly higher apoptotic percentage and lower living percentage than cells cultured on NP surface. (*C*) The apoptotic cells showed a significant decrease in spreading area. Rhodamine phalloidin staining showed the distribution of actin stress fibers (*D*), and the low intracellular fluorescent intensities indicated the loss of actin stress fibers (*E*) for apoptotic cells; the intensity of *p*-FAK (phosphorylated FAK) also decreased significantly in MP-15 cells (*F*). (*G*) EC staining by the Annexin V for cell membrane blebbing provides an early indicator of apoptosis. *, significant difference ($P < 0.05$) from NP; #, significant difference ($P < 0.05$) between two groups.

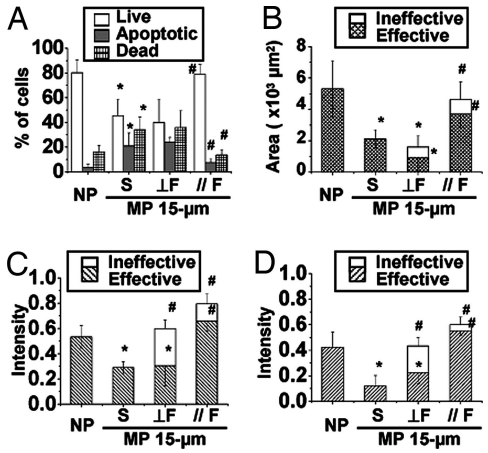

Fig. 2. Countering of constraint-induced EC apoptosis by parallel flow. After seeding on 15-μm strips (MP 15-μm) for 12 h, HUVECs were subjected to pulsatile flow (shear stress = 12 ± 4 dyn/cm^2) in a direction perpendicular (⊥F) or parallel (//F) to the long axis of the strips, or kept under static condition (S), for an additional 12 h. (*A*) Parallel flow led to a significant increase of living cells and reduction of apoptosis, whereas perpendicular flow did not. (*B*) Parallel flow also increased the cell spreading area to values similar to those for cells on NP surface; with perpendicular flow, most of the cell spreading area was outside the strip (ineffective). Both parallel and perpendicular flows increased the total fluorescent staining intensities of actin stress fibers (*C*) and *p*-FAK (*D*). (*C* and *D*) However, the effective intensities of stress fibers and *p*-FAK within the MP area were enhanced only in cells subjected to parallel, but not perpendicular, flow. *, significant difference ($P < 0.05$) from NP; #, significant difference ($P < 0.05$) in comparison with the MP 15-μm static condition.

stamp containing microfluidic channels [supporting information (SI) Fig. 7]. HUVECs cultured on nonpatterned (NP) surfaces have a random orientation and these HUVECs cultured on 60-, 30-, and 15-μm strips showed progressive increases in alignment with the direction of the strips (Fig. 1*A*). When compared with cells on NP surface, anisotropical confinement of HUVECs onto the 15-μm strips led to a significant decrease in the percentage of living cells and increase in the percentage of apoptotic cells, as shown by flow cytometry (Fig. 1*B*). The cell spreading areas on 15-μm strips also decreased significantly when compared with the cells on NP surface, as well as on 60- and 30-μm strips (Fig. 1*C*). The decrease in strip width caused a progressive decrease of the short axis, but no significant change in the long axis of ECs (SI Fig. 8*A*). These results indicate that we can modulate EC orientation and morphology and control cell fate by micropatterning FN to constrain cell spreading in one direction (width).

We assessed the cellular remodeling in terms of stress fiber formation and orientation (by labeling actin with rhodamine phalloidin) and FAK phosphorylation [by using an anti-*p*-FAK (Y397) antibody followed by a FITC conjugated secondary antibody]. The ECs on 15-μm strips had significantly lower intracellular intensity of rhodamine phalloidin than cells on 60- and 30-μm strips, as well as NP surface (Fig. 1 *D* and *E*), indicating a loss of actin stress fibers, which were transformed into strong cortical rings as an early indicator of apoptosis (Fig. 1*D*). The HUVECs cultured on 15-μm strips also showed a significant reduction of *p*-FAK (Fig. 1*F*). Histochemical examination with Annexin V-FITC staining confirmed the cell apoptosis (Fig. 1*B*), with membrane blebbing as an indication of early stage of apoptosis for HUVECs seeded on 15-μm strips (Fig. 1*G*), but not on 60- and 30-μm strips.

Parallel Flow Countered the Constraint-Induced Apoptosis. The application of pulsatile flow in a direction parallel to the strips was able to counter the apoptosis induced by anisotropic constraint on the 15-μm strips. Parallel flow caused a significant increase in living cells and a significant decrease of apoptotic cells (Fig. 2*A*); these values became similar to those for cells cultured on NP surfaces under static condition. The anti-apoptotic effect of parallel flow was confirmed by the lack of Annexin V-FITC staining (SI Fig. 9). In contrast, perpendicular flow did not stop the HUVECs from undergoing apoptosis on 15-μm strips. Parallel flow induced HUVEC elongation (SI Fig. 8*B*) and a significant increase of cell spreading area (Fig. 2*B* and SI Movie 1); perpendicular flow did not have such effects. Because the flow effects depend on cell adhesion to the matrix, we separate the cell spreading area into effective (inside the strips) and ineffective (outside the strips) parts. For ECs subjected to parallel flow, most of the cell area is within the strip (effective), but for ECs subjected to perpendicular flow, a significant portion of the cell is outside of the strip (ineffective) (Fig. 2*B*).

Rhodamine phalloidin staining showed that flow in either parallel or perpendicular direction caused an increase of stress fiber formation (Figs. 2*C* and 3 *A* and *B*). Time-lapse living cell images indicate that the cells had difficulty holding onto the area without MP (FN) under perpendicular flow as they could not establish focal adhesion sites, and they eventually peeled off (SI Movie 2). We determined the fluorescence intensities of stress

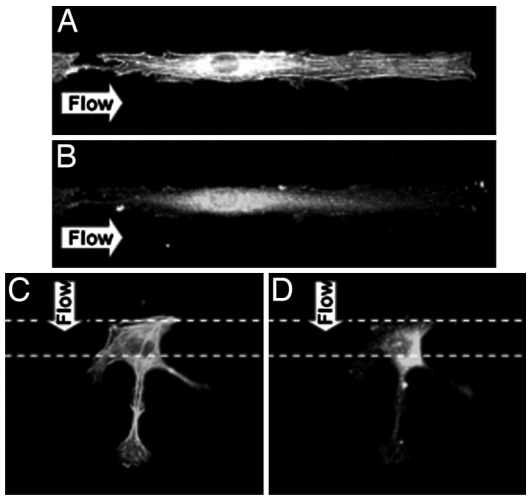

Fig. 3. HUVEC remodeling on MP strips under flow in different directions. Parallel flow increased the stress fiber formation for cytoskeleton remodeling (*A*) and *p*-FAK for the anchoring points at the ends of stress fibers (*B*). In contrast, the perpendicular flow increased the stress fibers (*C*) and *p*-FAK (*D*) in the ineffective NP surface and therefore mitigated the effectiveness of these inductions.

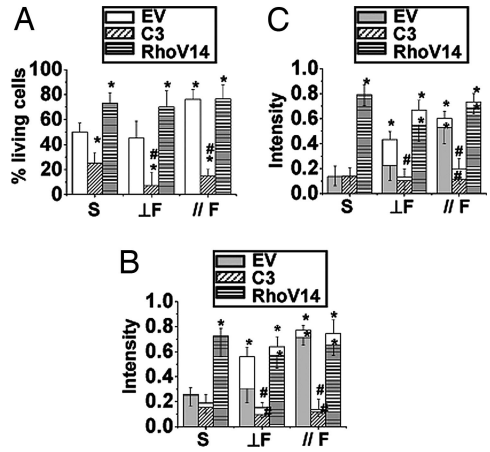

Fig. 5. Rho activities can dominate flow effects on apoptosis. HUVECs were transfected with empty vector (EV), C3 exoenzyme (C3), or RhoV14, followed by transferring onto 15-μm strips, and then subjected to parallel flow (//F), perpendicular flow (⊥F), or kept in static condition (S). Flow cytometry showed that C3-transfected cells had a significantly lower living cell percentage under static condition and abolished the antiapoptotic effect of parallel flow. In contrast, the transfection of RhoV14 significantly reduced the percentage of apoptotic cells under static condition (*A*). RhoV14-transfected cells showed significant increases of the effective intensities of stress fibers (*B*) and *p*-FAK (*C*) under both directions of flow and static condition. *, significant difference ($P < 0.05$) compared with EV under static condition; #, significant difference ($P < 0.05$) compared with EV under the same flow condition.

fibers and *p*-FAK inside (effective) and outside the strips (ineffective). Although perpendicular flow caused an increase in the total intensity of stress fibers in ECs on 15-μm strips over the control static cells, there was no increase of the effective intensity (Figs. 2*C* and 3*C*). In contrast, parallel flow caused significant increases of both the total and effective intensities of stress fibers. Parallel flow also induced the remodeling of focal adhesion site, as indicated by total and effective *p*-FAK staining (Figs. 2*D* and 3*B*) compared with static control (Fig. 4*D*). Perpendicular flow enhanced the total intensity of *p*-FAK in comparison to static cells on 15-μm strips, but not the effective intensity (Figs. 2*D* and 3*D*).

Rho GTPase Prevented the Constraint-Induced Apoptosis. We examined the role of Rho small GTPase in regulating the actin cytoskeleton and focal adhesions, and hence its effects on the apoptosis induced by anisotropic constraint and stoppage by parallel flow.

Role of Rho GTPase under static condition. The transfection of His–tagged C3 (10 μg/ml) resulted in the expression of Rho-inhibitory C3 in the cytosol (verified by immunostaining of His-tag, SI Fig. 10), the disassembly of actin stress fibers, and the inhibition of *p*-FAK (Fig. 4*B*). In contrast, the transfection of cells with RhoV14 (constitutively active Rho) enhanced stress fiber formation and *p*-FAK (Fig. 4*C*). The transfected cells were transferred onto the 15-μm strips for another 12 h and then fixed for the examinations of stress fiber formation, *p*-FAK distribution, and apoptosis (Fig. 4 *D–F*). The C3-treated cells did not have well-defined cell borders on the edge of the MP strips and nor *p*-FAK staining (Fig. 4*E*). In contrast, the RhoV14-transfected cells on the 15-μm strips showed enhancements of stress fiber formation and *p*-FAK staining at the anchor spots (Fig. 4*F*). Flow cytometry analyses showed that C3-transfection caused a significant decrease of living cells on 15-μm strips in comparison to cell transfected with empty vector (EV) (Fig. 5*A*). The transfection of C3 or RhoV14 did not cause any significant changes in cell spreading area, nor cell lengths in long/short axes (SI Fig. 11). In contrast to C3 exoenzyme, however, the RhoV14-transfection not only restored the cytoskeleton (Fig. 5*B*) and focal adhesions (Fig. 5*C*), but also significantly reduced the

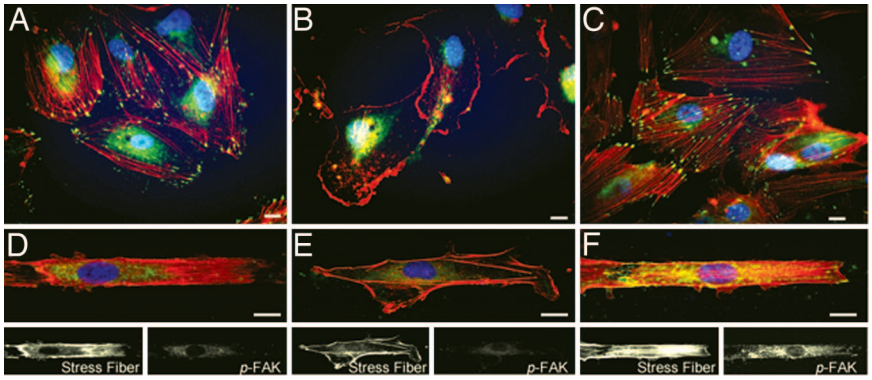

Fig. 4. Rho activates *p*-FAK and restores actin cytoskeleton of constrained ECs under static condition. Shown are confocal images for HUVECs transfected with empty vector control (*A* and *D*), C3 exoenzyme (*B* and *E*), or RhoV14 (*C* and *F*) on NP surfaces (*A–C*) and 15-μm strips (*D–F*). Cells were immunostained for *p*-FAK (green), rhodamine phalloidin (red), and Hoechst (blue). (Scale bar: 15 μm.)

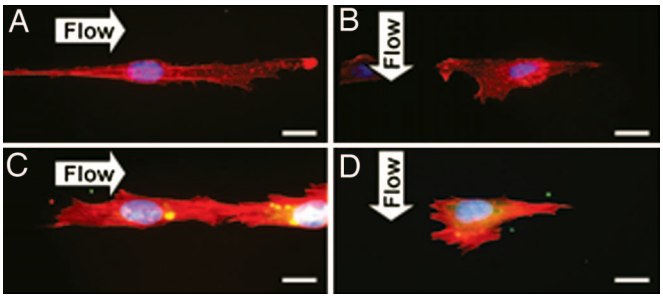

Fig. 6. Rho activities attenuate constraint-induced apoptosis and enable cytoskeleton remodeling independent of flow direction. Shown are images for HUVECs transfected with C3 exoenzyme (*A* and *B*) or RhoV14 (*C* and *D*) on 15-μm strips, and then subjected to parallel (*A* and *C*) or perpendicular (*B* and *D*) flow. The inhibition of Rho activities abolished the antiapoptotic effect of parallel flow and blocked the formation of stress fibers (*A*); RhoV14 attenuated constraint-induced cell apoptosis and restored the actin cytoskeleton under both flow directions (*C* and *D*). Cells were immunostained in the same method as Fig. 4. (Scale bar: 15 μm.)

constraint-induced apoptosis and improved survival on 15-μm strips under static condition (Fig. 5*A*).

Role of Rho GTPase under flow conditions. C3 treatment abolished the anti-apoptotic effect of parallel flow (Fig. 5*A*), and resulted in the loss of the C3-transfected cells under both parallel and perpendicular flows. In contrast, the transfection of RhoV14 reduced the HUVECs apoptosis under both directions of flows (Fig. 5*A* and SI Fig. 12). The prevention of apoptosis by RhoV14 transfection did not change their morphology under both flow directions (SI Fig. 11). Immunostaining showed that C3 abolished the stress fibers and *p*-FAK under static (Fig. 4 *B* and *E*) and both flow directions (Fig. 6 *A* and *B*). In contrast, RhoV14 increased the intensities of stress fibers and *p*-FAK under static (Fig. 4 *C* and *F*) and both flow conditions (Fig. 6 *C* and *D*). The effective intensities of stress fibers (Fig. 5*B*) and *p*-FAK (Fig. 5*C*) were significantly enhanced in RhoV14-transfected cells under both directions of flow; this enhancement is especially noteworthy for perpendicular flow, which did not increase these effective intensities, nor did it stop apoptosis in the absence of RhoV14. Hence, the results suggest that the increases in Rho activation can override the anisotropic constraint-induced apoptosis and also eliminate the direction-dependency of the flow-reversal of apoptosis on constrained surface.

Discussion

We hypothesize that the attachment of ECs to ECM and the consequent changes in stress fibers, focal adhesions, and intracellular mechanics provide the survival signal and that the anisotropic constraint-induced apoptosis is attributable to the loss of this cell adhesion-induced signaling. When the short axis of the EC was constrained by the 15-μm strips, the limited elongation in the long axis (SI Fig. 8*A*) cannot provide a sufficient compensation in cell adhesion area (Fig. 1*C*), and the consequent reductions of stress fiber formation (Fig. 1*E*) and FA complex (Fig. 1*F*) are probably the cause for cell apoptosis. We coated strip surfaces with different FN concentrations (10–40 μg/ml), but increases of FN concentration could not prevent the apoptosis (data not shown), suggesting that the increase of apoptosis in narrow strips is mainly due to anisotropic constraints and the consequent alterations in stress fibers and focal adhesions on the cell side, rather than insufficient FN binding sites on the matrix side.

Apoptosis is more prone to occur in cell types that are unable to spread out to form firm matrix attachments and stress fibers, e.g., fibroblasts, epithelial cells, and ECs (6–8). The progression of apoptosis in these cells has been shown to involve the disassembly of the FA complexes and the reassembly of actin into a peripheral ring, and the consequent bleb formation (9). In the present study, the apoptotic HUVECs on 15-μm strips under static condition also displayed the cortical actin ring (Fig. 1D), loss of FA complex (Fig. 4*D*), and membrane blebbing by staining of either the actin stress fibers (Fig. 1*D*) or Annexin V (Fig. 1*G*), which is one of the earliest indications of apoptosis.

The survival of ECs is intimately tied to their local microenvironment. Our data indicate that shear force can modify the actin cytoskeleton and the anchoring FA and that the direction of flow can modulate the effectiveness of the flow-induced remodeling, thus modulating the cell surviving signals. It has been shown that the elongated cell morphology induced by anisotropic mechanical inputs causes the anisotropic distribution of cytoskeleton to result in mechanical anisotropy and deformation pattern (10). There is also evidence that the cell traction force is correlated with cell morphology, especially the cell width in smooth muscle cells (11), and cytoskeleton formation (12). Together, the results in the present study and those in the literature suggest that the interrelationships among traction force, cytoskeletal formation/stability, and cell morphology play an important role in regulating cell survival. In the current study, we demonstrated that parallel flow can promote cytoskeletal and FA remodeling and counter apoptosis (Fig. 2). In contrast, the perpendicular flow, which cannot induce effective remodeling, cannot counter the apoptosis on the 15-μm strips in the absence of an enhancement of Rho activity. Our results further demonstrated that the HUVECs interact with both the ECM-environment (which was manipulated with anisotropically micropatterned FN) and the mechanical environment (which was altered by shear flows in different directions) to modulate EC fates.

The Rho family small GTPases have distinct functions in regulating the actin-based cytoskeletal structure (13), focal adhesions (14), as well as apoptosis (15). Integrin and Rho GTPases are intimately connected at multiple levels (for review, see ref. 16). It has been shown that Rho causes the tyrosine phosphorylation of FAK to augment the onset of stress fiber formation (17). Treatment of HUVECs with the RhoA kinase inhibitor Y-27632 causes dose-dependent cell death (15). Similar cell apoptosis occurs after the blockade of RhoA function by exoenzyme C3, which markedly decreases the basal phosphorylation state of FAK (14). Rho has also been shown to be a mediator of mechanical signaling (18). By using the Rho affinity pull down assay, shear flow has been found to cause a transient suppression in RhoA activity followed by a modest activation (19). The inhibition of RhoA with C3 exoenzyme abolishes the shear-induced EC alignment and EC migration (20).

Our results showed that the inhibition of Rho with C3 abolished the stress fiber formation, FA assembly, and the anti-apoptotic effect of parallel flow in ECs subjected to geometric constraint (Fig. 5*A*). On the other hand, constitutively active Rho (RhoV14), which enhanced cytoskeleton-FA formation in HUVECs seeded on 15-μm strips (Fig. 4*F*), prevented the anisotropic constraint-induced apoptosis under static condition in a dose-dependent manner (SI Fig. 13). It is to be noted that the anti-apoptotic effect of RhoV14 was not accompanied by a change in cell morphology, as in the case of the anti-apoptosis by parallel flow. In fact, RhoV14 caused a significant inhibition of cell elongation in the direction of flow and a slight reduction in the short axis as compare to cells transfected with empty vector or C3 (SI Fig. 11). Furthermore, RhoV14 had anti-apoptotic effects under both perpendicular and parallel flows. One way to explain these findings is that both parallel flow and RhoV14 exert their anti-apoptotic effects through the formation/organization of cytoskeleton-FA and the consequent changes in intracellular mechanics. The effect of RhoV14 is probably much stronger than that of flow such that RhoV14 is anti-apoptotic

even under perpendicular flow. Our previous studies on ECs subjected to cyclic uniaxial stretch showed that the Rho-mediated stress fiber reorganization is critical in the adaptive changes in intracellular mechanics and signaling that are protective against apoptosis (18, 21). Therefore, our studies using different ways to alter the extracellular environment, including stretch, shear, and geometric constraint, point to a unified concept that the Rho-mediated organization of stress fibers and focal adhesions, and the consequent change in intracellular mechanics, constitute a feedback mechanism to maintain cell integrity in the face of external stimuli.

In summary, we demonstrated that the anisotropic constraint of HUVEC culture on MP strips caused alterations in cell morphology and survival status. HUVECs seeded on 15-μm strips showed significant decreases of spreading area and survival rate with losses of stress fibers and focal adhesions. The application of parallel flow had an anti-apoptotic effect against anisotropic constraint by increasing the effective cell spreading area and by enhancing stress fibers and *p*-FAK in intracellular signaling, thus improving cell survival. Perpendicular flow had little effect on effective intracellular organization, and thus was not able to counter the anisotropic constraint-induced apoptosis. We also demonstrated that Rho GTPase plays an important role in the constraint-induced EC apoptosis. The inhibition of Rho abolished the anti-apoptotic effect of parallel flow, whereas the constitutively active Rho was able to prevent cell apoptosis regardless of the presence or the direction of flow. These results suggest that the orchestration of the mechanisms regulating cell fate involves interplays of cell morphology and external forces, leading to changes in intracellular signaling events, formation/organization of stress fibers and focal adhesions to modify intracellular mechanics, culminating in the modulation of cell fate.

Materials and Methods

Cell Culture. HUVECs were cultured before passage 10 in M199 (Invitrogen, Carlsbad, CA) supplemented with 20% FBS (HyClone, Logan, UT), 20% endothelial growth medium (Cell Application, San Diego, CA), and 1% penicillin–streptomycin, and maintained in a humidified incubator at 37°C with 5% CO_2.

Constraining Cell Morphology by MP Strips. The modified methods of injection PDMS (Sylgard 184; Dow Corning, Midland, MI) stamp were used as described (5). Strips of FN with different widths (15, 30, and 60 μm) were created on a silicon membrane by using a PDMS stamp containing microfluidic channels (SI Fig. 7). The PDMS stamp was made by replica casting PDMS against a master made by photolithography and cured at 65°C for 2 h in a vacuum chamber. The master was created by spin-coating a 100-μm layer of SU-8 100 negative tone photoresist material (MicroChem, Newton, MA), followed by the processing of SU-8 fabrication steps: soft baking, exposure, postexposure baking, and development. After development, the positive mold of photoresist material was silanized with fluorosilane [(tridecafluoro-1,1,2,2-tetrahydrooctyl)-1-trichlorosilane; United Chemical Technologies, Bristol, PA] for 1 h to aid the subsequent release of PDMS. As the PDMS cured and peeled off, microfluidic channels with different widths were created and connected by polyethylene tubes for injecting the ECM.

The silicon rubber membrane (Specialty Manufacturing, Saginaw, MI) that had been treated by UV was held by a chamber holder as described (18), and a glass slide was inserted on the bottom surface to support the membrane. The PDMS stamp with microfluidic channels was then placed on the upper surface of the membrane and injected with FN solution (20 μg/ml; Sigma–Aldrich, St. Louis, MO) for adsorption for 4 h. After FN deposition, the PDMS stamp was peeled off and the membrane was rinsed thoroughly with PBS (Invitrogen). To protect the silicone membrane surface without MP from protein adsorption and cell adhesion, the nonpatterned area was blocked by 0.2% (wt/vol) Pluronic F108 (Mount Olive, NJ) in PBS for 1 h and carefully rinsed with PBS without allowing the surface to dry. We used the hydrophobic polypropylene segment to stabilize Pluronic onto the surface by means of hydrophobic interactions, whereas the two polyethylene segments extend into the bulk aqueous medium (22). The wettability of silicone rubber is more suitable for protein deposition and provides better defined areas for cell adhesion (23). Micropatterning the FN on silicone membrane provided better confinement of cell area than only silanizing the glass surface when we combined this approach with shear stress application (data not shown). Silicon membranes with the whole surface coated with FN (nonpatterned, NP) were also made.

HUVECs were seeded on the MP strips for 30 min, and the nonadhered cells were washed away by changing medium. The attached cells were cultured in an incubator for 12 h and then used for flow experiments or kept in static condition.

Pulsatile Shear Flow. The MP strip containing the cultured cells was assembled into a flow chamber (20). A pulsatile flow with a shear stress of 12 $\pm$ 4 dyn/cm^2 was applied in the direction perpendicular or parallel to the long axis of the strips. Superimposed on the mean value of 12 dyn/cm^2 was a sinusoidal oscillation with a frequency of 1 Hz and a peak-to-peak amplitude of $\pm$4 dyn/cm^2, which was created by connecting a piston pump to the hydrostatic flow system. The parameters of the pulsatile flow were chosen on the basis of estimated arterial wall shear stress. Concurrent experiments were performed on cells kept in the flow chamber under static condition for the same duration as the flow experiments. The pH of the medium was maintained constant by gassing with a mixture of 5% CO_2 and 95% air, and the temperature was maintained at 37°C.

Flow Cytometry. The Annexin V-FITC apoptosis detection kit (BD Biosciences, San Jose, CA) was used to stain apoptotic cells. The stained cells were analyzed by using flow cytometry (Becton Dickinson). In brief, HUVECs seeded on MP strips, as well as NP surface, were washed twice with cold PBS, trypsinized, and resuspended in 1$\times$ binding buffer at a concentration of 1×10^5 cells per ml. Annexin V-FITC (9×10^{-3} μg/μl) and propidium iodide (PI) (2.27×10^{-3} μg/μl) were added to the cell suspension (100 μl), followed by incubation for 15 min at room temperature. Four hundred microliters of 1$\times$ binding buffer was added to the stained cell suspension. The cells in the population were identified as living cells [Annexin V-FITC (−), PI (−)], early apoptotic cells [Annexin V-FITC (+), PI (−)], and late apoptotic or dead cells [Annexin V-FITC (+), PI (+)]. At least 10,000 cells were analyzed by using flow cytometry for each group in each experiment to assess the cell fates in the population of cells seeded on MP surfaces. The numbers of living and apoptotic cells were calculated and normalized to the total cell number determined under static condition.

Rho Family Protein Transfection. The His-tagged *Clostridium botulinum* C3 exoenzyme (C3, which inhibits RhoA, RhoB, and RhoC functions; 10 μg/ml) was transfected into HUVECs by using Lipofectamine 2000 (Invitrogen) to inhibit Rho activity. The GST-tagged RhoV14 protein (20 μg/ml) was transfected into HUVECs to enhance Rho activity. After transfection for 12 h, the cells were transferred to the MP strips for another 12 h, followed by the application of parallel or perpendicular flow for an additional 12 h. The anti-His (1:200; Santa Cruz Biotechnology, Santa Cruz, CA) and anti-GST (1:200; Santa Cruz Biotechnology) antibodies were used to detect the transfected proteins to assure high transfection efficiency.

Immunostaining. The cells were fixed with 4% paraformaldehyde (Sigma–Aldrich), permeabilized in 0.1% Triton X-100 (Sigma–Aldrich), and blocked with 1% horse serum (Invitrogen) in PBS for 30 min. The phosphorylation of FAK was detected by using mouse monoclonal anti-*p*-FAK (Y397) antibody (1:200; BD Transduction Laboratories, Lexington, KY) followed by the FITC-conjugated anti-mouse secondary antibody (1:200; Jackson ImmunoResearch Laboratories, West Grove, PA). The stress fibers were stained with rhodamine phalloidin (1:200; Molecular Probes, Eugene, OR), and cell nuclei were visualized with Hoechst staining (1:1,000; Molecular Probes). After immunostaining, the sample was washed with PBS and mounted in VECTASHIELD mounting medium (Vector Laboratories, Burlingame, CA).

Time-Lapse and Confocal Microscopy. The time-lapse phase contrast images (×20 objective) were collected with a cooled CCD camera (Orca II ER; Hamamatsu Photonics, Hamamatsu City, Japan) at 10-min intervals and transferred from a frame grabber to computer storage by using an inverted microscope (Olympus, Tokyo, Japan). The confocal microscope (Olympus) with ×40 oil objective lens, a cooled CCD camera, and system control software (MetaMorph, Downingtown, PA) was used to measure the 3D structure of stress fibers and the distribution of *p*-FAK. Images of 1-μm-thick sections were collected from bottom to top of the cell for each field.

Cell morphology was analyzed by using an image processing program (MATLAB; MathWorks, Natick, MA) to determine the orientation, lengths of long/short axes, and spreading area of the cells. The outline of each cell was determined from phase contrast images. The contour was fit to an ellipse, and the angle of orientation of the major axis of the ellipse was determined as described (24). Cell orientation was determined as the angle (θ) between the long axis of the cell and the longitudinal axis of the MP strip. Cell spreading area is calculated by the image pixels inside the cell contour with the calibration of image scale for converting pixel size into length scale (micrometers). The average intracellular fluorescent intensities of actin stress fibers and *p*-FAK were calculated by using a gray scale from 0 to 1 (0, black; 1, white). The intracellular cytoplasmic area was defined after removing the peripheral cortical border by threshold imaging (or manual drawing) for each individual cell. For cells subjected to flow stimulation, the effective intensities were also measured for the immunostained protein within the areas of the FN strips in addition to those in the total cell spreading area. At least 30 cells were randomly selected and analyzed in each experiment.

Statistical Analysis. Data represented are mean ± standard error from three independent experiments for each treatment group. The differences between groups were analyzed by one-way ANOVA and Bonferroni test for multiple comparisons, with $P < 0.05$ taken as statistically significant.

Support for this research was provided by National Institutes of Health Grants HL-064382, HL-080518, and HL-085195.

1. Cines DB, Pollak ES, Buck CA, Loscalzo J, Zimmerman GA, McEver RP, Pober JS, Wick TM, Konkle BA, Schwartz BS, *et al*. (1998) *Blood* 91:3527–3561.
2. Chen CS, Mrksich M, Huang S, Whitesides GM, Ingber DE (1997) *Science* 276:1425–1428.
3. Li YS, Haga JH, Chien S (2005) *J Biomech* 38:1949–1971.
4. Ingber DE (2002) *Circ Res* 91:877–887.
5. Li S, Bhatia S, Hu YL, Shiu YT, Li YS, Usami S, Chien S (2001) *Biorheology* 38:101–108.
6. Brancolini C, Lazarevic D, Rodriguez J, Schneider C (1997) *J Cell Biol* 139:759–771.
7. Levkau B, Herren B, Koyama H, Ross R, Raines EW (1998) *J Exp Med* 187:579–586.
8. Huot J, Houle F, Rousseau S, Deschesnes RG, Shah GM, Landry J (1998) *J Cell Biol* 143:1361–1373.
9. Mills JC, Stone NL, Pittman RN (1999) *J Cell Biol* 146:703–708.
10. Hu S, Eberhard L, Chen J, Love JC, Butler JP, Fredberg JJ, Whitesides GM, Wang N (2004) *Am J Physiol* 287:C1184–C1191.
11. Tolic-Norrelykke IM, Wang N (2005) *J Biomech* 38:1405–1412.
12. Dembo M, Wang YL (1999) *Biophys J* 76:2307–2316.
13. Hall A (1998) *Science* 279:509–514.
14. Bobak D, Moorman J, Guanzon A, Gilmer L, Hahn C (1997) *Oncogene* 15:2179–2189.
15. Li X, Liu L, Tupper JC, Bannerman DD, Winn RK, Sebti SM, Hamilton AD, Harlan JM (2002) *J Biol Chem* 277:15309–15316.
16. Tzima E (2006) *Circ Res* 98:176–185.
17. Ishizaki T, Naito M, Fujisawa K, Maekawa M, Watanabe N, Saito Y, Narumiya S (1997) *FEBS Lett* 404:118–124.
18. Kaunas R, Nguyen P, Usami S, Chien S (2005) *Proc Natl Acad Sci USA* 102:15895–15900.
19. Wojciak-Stothard B, Ridley AJ (2003) *J Cell Biol* 161:429–439.
20. Hsu PP, Li S, Li YS, Usami S, Ratcliffe A, Wang X, Chien S (2001) *Biochem Biophys Res Commun* 285:751–759.
21. Kaunas R, Usami S, Chien S (2006) *Cell Signal* 18:1924–1931.
22. Bohner M, Ring TA, Rapoport N, Caldwell KD (2002) *J Biomater Sci Polym Ed* 13:733–746.
23. Tan JL, Liu W, Nelson CM, Raghavan S, Chen CS (2004) *Tissue Eng* 10:865–872.
24. Galbraith CG, Skalak R, Chien S (1998) *Cell Motil Cytoskeleton* 40:317–330.